

See discussions, stats, and author profiles for this publication at: <https://www.researchgate.net/publication/269173349>

Influence of Geometric Patterns of Microstructured Superhydrophobic Surfaces on Water-Harvesting Performance via Dewing

ARTICLE in LANGMUIR · DECEMBER 2014

Impact Factor: 4.46 · DOI: 10.1021/la5041486 · Source: PubMed

CITATIONS

2

READS

28

3 AUTHORS, INCLUDING:



Choongyeop Lee

Kyung Hee University

18 PUBLICATIONS 439 CITATIONS

SEE PROFILE

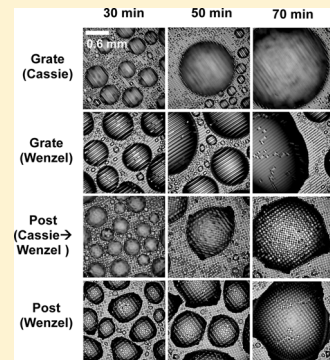
Influence of Geometric Patterns of Microstructured Superhydrophobic Surfaces on Water-Harvesting Performance via Dewing

Donghyun Seo,[†] Choongyeop Lee,^{*,‡} and Youngsuk Nam^{*,†}

[†]Department of Mechanical Engineering, Kyung Hee University, Yongin 446-701, Korea

[‡]School of Aerospace and Mechanical Engineering, Korea Aerospace University, Goyang 412-791, Korea

ABSTRACT: On superhydrophobic (SHPo) surfaces, either of two wetting states—the Cassie state (i.e., nonwetted state) and the Wenzel state (i.e., wetted state)—can be observed depending on the thermodynamic energy of each state and external conditions. Each wetting state leads to quite a distinctive dynamic characteristic of the water drop on SHPo surfaces, and it has been of primary interest to understand or induce the desirable wetting state for relevant thermofluid engineering applications. In this study, we investigate how the wetting state of microstructured SHPo surfaces influences the water-harvesting performance via dewing by testing two different patterns, including posts and grates with varying structural parameters. On grates, the observed Cassie wetting state during condensation is well described by the thermodynamic energy criteria, and small condensates can be efficiently detached from the surfaces because of the small contact line pinning force of Cassie droplets. Meanwhile, on posts, the observed wetting state is dominantly the Wenzel state regardless of the thermodynamic energy of each state, and the condensates are shed only after they grow to a sufficiently large size to overcome the much larger pinning force of the Wenzel state. On the basis of the mechanical force balance model and energy barrier consideration, we attribute the difference in the droplet shedding characteristics to the different dynamic pathway from the Wenzel state to the Cassie state between posts and grates. Overall, the faster droplet shedding helps to enhance the water-harvesting performance of the SHPo surfaces by facilitating condensation on the droplet-free area, as evidenced by the best water-harvesting performance of grates on the Cassie state among the tested surfaces.



1. INTRODUCTION

The condensation behavior on micro/nanostructured hydrophobic surfaces, so-called superhydrophobic (SHPo) surfaces, has been a subject of great interest because of the potential for increasing the heat- and mass-transfer performances in energy and environmental applications including power generation, water harvesting, thermal management, and air conditioning.^{1–5} Previous studies have reported that the condensates on SHPo can be easily removed by gravitational forces or coalescence-induced jumping mainly as a result of the minimized contact line pinning and viscous dissipation.^{6,7}

Many studies have demonstrated that the condensation characteristics are dependent on the geometry of micro/nanostructures in a way in which the geometric details influence the nucleation site and rate of condensates.^{8–10} Moreover, it was found that drops could interact with the surface structures in two different ways: that is, the drop may sit on the top of surfaces structures with a vapor layer underneath (i.e., the Cassie state) or the drop may homogeneously wet the structured surface (i.e., the Wenzel state).¹¹ Please note that the Cassie state is associated with the high drop mobility because of the reduced contact area between the water and the solid, and the Wenzel state incurs reduced drop mobility due to the increased contact area between the water and solid.⁹ The two different wetting states can be observed even on the same SHPo surface, as one wetting state transitions to another

wetting state,^{12,13} and the resulting wetting state would hold significance in various hydrodynamic applications including drag reduction,^{14–17} liquid transportation,^{18–20} and droplet sliding.^{21,22}

Recently, water harvesting from air-borne moisture has received renewed interest as a promising way to address the global water shortage problem, with improved understanding of the role of micro/nanostructures residing on moisture harvesters in nature.^{23,24} Although the main interest has been directed to the understanding of surface structures in more common fog harvesters, it was recognized a long time ago that another viable way to harvest water from air is via dewing (or condensation).^{25,26} Actually, a water-harvesting strategy from dew is adopted in certain species, such as green tree frogs, *Litoria caerulea*, and the Namibian beetle, *Physasterna cribripes*,^{23,27} and it is believed that the wettability and surface structures of these species play an important role in water collection from dew.²³

The recent experimental study showed that the amount of the harvested water from dew varies with the wetting characteristics of surfaces.²⁸ However, the previous work focused only on the influence of macroscopic contact angles

Received: October 20, 2014

Revised: November 30, 2014

Published: December 2, 2014

without taking into account the effects of the microscopic geometrical details. Accordingly, our goal in this study is to clarify the influence of microscopic structural features on the dew-harvesting performance by elucidating the dynamic interaction between surface structures and condensates during condensation. In this study, we limit our attention to SHPo surfaces for several reasons. First, a hydrophilic surface would be more easily contaminated by air-borne particles or pathogens^{10,29} after some time because of its high surface energy, which might raise the contamination issue of the harvested water, whereas the SHPo surface would be relatively free from this issue because of its self-cleaning ability. Second, the effects of surface structures are more profound on SHPo surfaces because drops could interact with the surface structures in different ways, including Cassie and Wenzel states that provide very different wetting morphologies. Finally, depending on applications, we might benefit from the enhanced heat-transfer performance of the SHPo surface while achieving water harvesting from dew at the same time.

To gain a better qualitative understanding of the difference in dew-harvesting performance among different surface structures, we devised a more specific measuring method that enables us to quantify both the frequency and mass of the collected droplets, unlike other studies that just measured the total mass of collected water over the test duration.^{28,30–32} In addition, instead of employing macroscopic properties such as the apparent contact angle and contact angle hysteresis for the calculations,^{28,31–33} we directly used the microscopic geometric information in modeling the interfacial dynamics of the water drop on the SHPo surfaces to clarify the influence of the structural features of SHPo surfaces on the dew-harvesting performance.

As surface structures, microscale grates and posts with varying structural parameters were selected for their simple geometry suitable for fundamental studies as well as their universality in natural surfaces.²³ Each structural parameter for the surfaces was determined on the basis of the thermodynamic energy criteria of each wetting state (i.e., the Cassie and Wenzel states) in such a way that one wetting state is favored over another wetting state with respect to energy consideration.¹⁰ To quantify the harvesting performance, both the mass and frequency of each collected droplet were measured under a temperature- and humidity-controlled environment and were used to correlate with the interfacial dynamics of the water drop on each surface.

Our results show that, with the highest drop mobility, Cassie state grates exhibit the best water-harvesting performance among the tested structures, illuminating the importance of the dynamic interactions of condensates with surface structures on the dew-harvesting performance. The thermodynamic energy analysis based on the macroscopic contact angles could not accurately capture the transition between the Cassie and Wenzel states, which shows the significance of the direct force and energy analyses using the microscopic geometric information.

2. EXPERIMENTAL METHODS

2.1. Design and Fabrication of Structured Surfaces. We fabricate surfaces with microscale post or grate structures on a silicon substrate using photolithography, followed by dry etching using the inductively coupled plasma (ICP) process. After the oxygen plasma treatment, the sample is functionalized with TFTS (trichloro-(1H,1H,2H,2H-perfluorooctyl)silane, Sigma) through the vapor

deposition process. Schematic images of surface structures are shown in Figure 1 along with detailed geometric parameters of the

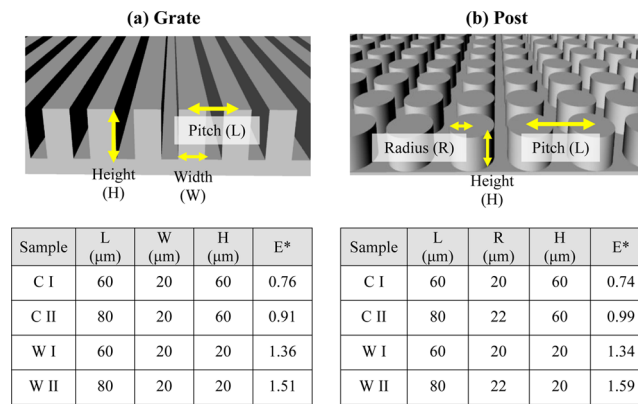


Figure 1. Schematic images of surface structures along with geometric parameters tested in the present study. C and W indicate the Cassie and Wenzel states, respectively.

investigated samples. The roughness factor r (i.e., the ratio of the actual surface area to the projected area) and solid fraction φ_s (i.e., the fraction of the top area of the total projected area) were calculated from the geometric information given in Figure 1. The normalized energy E^* is defined as $E^* = (\cos \theta_a^{CB}/\cos \theta_a^W) = (-1/r \cos \theta_a)$ to determine the thermodynamically favorable wetting morphology between Cassie and Wenzel states.¹⁰ With θ_a being the advancing contact angle of a smooth surface, when $E^* < 1$, a drop is thermodynamically favored to be in the Cassie state; otherwise, a drop is expected to be in the Wenzel state.^{10,12,34} Please note that, in calculating E^* , we used the advancing contact angle following the previous study¹⁰ which demonstrated that E^* based on the advancing contact angle can successfully capture the experimentally observed wetting states during condensation. On the basis of E^* calculated with the measured advancing contact angle of 116° on the smooth surface treated with TFTS, we designed surface structures with a thermodynamic preference either for the Cassie state (denoted as grate-C or post-C in this study) or the Wenzel state (denoted as grate-W and post-W).

2.2. Water-Harvesting Test. The experimental setup used for collecting water is shown in Figure 2. Each sample (3 cm × 3 cm size and 0.5 mm thickness) was tested within the environmental chamber where the temperature and humidity were set to be 27.0 ± 3.0 °C and 90–95%, respectively. The investigated sample was placed vertically on the cooling module. Water at 10 °C from a thermal bath was circulated into a cold plate to maintain the sample temperature at 12.5 ± 0.1 °C. The hot vapor generated from boiling water was supplied into the environmental chamber to maintain the high humidity level. To prevent direct contact between vapor droplets and the test surface (i.e., to observe the water harvesting only via dewing), the vapor inlet was placed behind the tested sample surface. During the experiments, the supersaturation level, $S = P_v/P_{sat}(T_s)$, was maintained at ~ 2.2 , where P_v is the vapor pressure, T_s is the surface temperature, and $P_{sat}(T_s)$ is the saturation pressure at T_s .

After the temperature and humidity reached equilibrium, the sample was installed into the cold plate to initiate water collection. While the water dripping from the sample was collected in a clean vessel, we checked the mass and time of each fallen droplet using an electronic scale and a stopwatch. Because condensation occurred everywhere during the measurement, the condensed water in unintended places such as the cold plate, water circulating hoses, and chamber walls was blocked from entering the collecting vessel to ensure that all of the collected water was from the test surface. The dynamic behavior of droplets was captured using a high-speed CCD camera (Phantom, M-110 with Nikon, AF Micro Nikkor 60 mm lens) installed in front of the chamber.

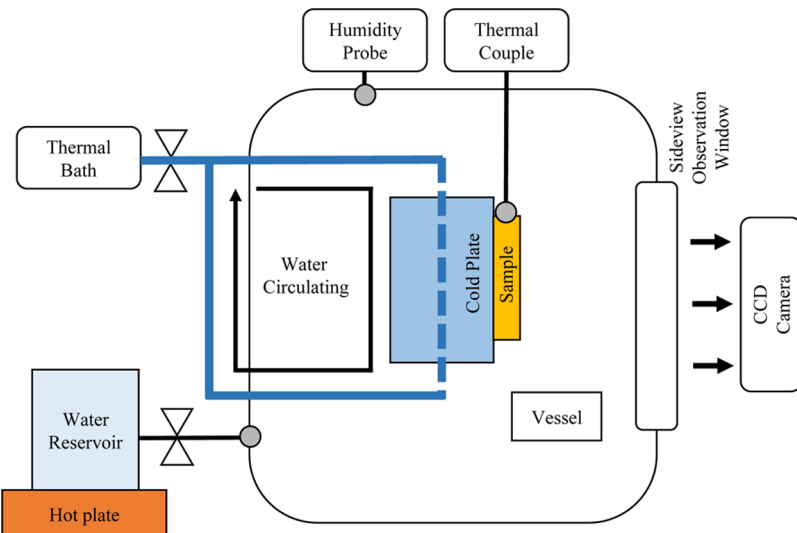


Figure 2. Schematic of the experimental setup used for the water-harvesting test.

3. RESULTS AND DISCUSSION

3.1. Sliding Behaviors of Condensed Droplets. Figure 3 shows the behavior of water condensation on each test surface,

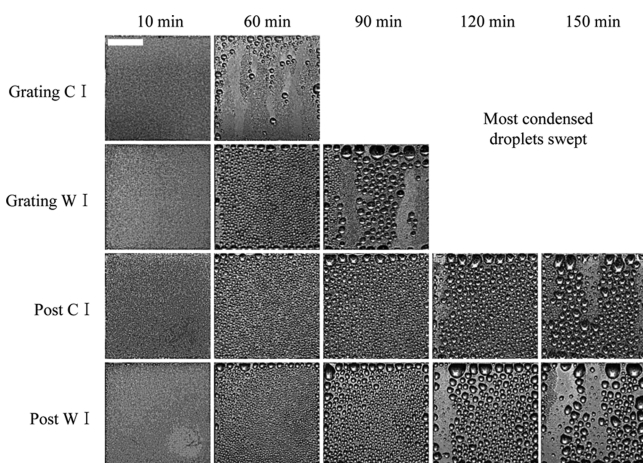


Figure 3. Time-lapse images of the water condensation on grate-C I, grate-W I, post-C I, and post-W I. On the grate surfaces, small droplets of less than 3 mm in diameter are removed from the surface after 60–120 min. Meanwhile, on the post surfaces, relatively large droplets (more than 5 mm in diameter) remain on the surface even after more than 150 min (scale bar = 10 mm).

captured using a CCD camera on the macroscale. Because of their hydrophobic nature, all surfaces exhibit high contact angles ($>130^\circ$) as well as a dropwise condensation mode. The droplets grow on the surface and then coalesce with adjacent droplets. When the droplets grow large enough to overcome the pinning force from the surface, they roll down the surface by gravity while sweeping the surface and merging with other droplets along their path. Then the droplets begin to grow again on the refreshed area.³⁵

In Figure 3, initially (10 min), the condensation behavior appears to be similar on all test surfaces because of the similar surface wettability. However, over time, a clear difference in the condensate morphology appears among test surfaces. For example, a closer look at the surface shows that the sizes of the pinned droplets are different among the investigated

surfaces,^{28,36} which might be attributed to the different pinning force on each surface. On grate-C I, most of the surface area is clear of droplets, and the average size of pinned droplets appears to be less than 1–3 mm in diameter, which is noticeably smaller than those (3–4 mm in diameter) on grate-W I. The difference can be explained by the fact that the mobility of droplets in the Cassie state is higher than that of droplets in the Wenzel state because of the smaller contact area between the water and the solid, and thus droplets on the Cassie state can be more quickly removed from the surface by gravity compared to droplets on the Wenzel state. Interestingly, we do not observe any difference in condensation behavior between post-C I and post-W I in contrast to grates. Moreover, the size of the remaining droplets on posts is mostly above 4–5 mm in diameter, which is larger than those on grates.

The different condensation behaviors on each test surface are closely related to the dynamic motion of droplets on each surface, as shown in Figure 4. Figure 4 shows that the size of the sweeping droplet on grate-C I (~2 mm in diameter) is smaller than that (~3.5 mm in diameter) on grate-W I, whereas the size of the sweeping droplet (~5 mm in diameter) is notably larger on posts than on grates, in agreement with Figure 3. On post-C and post-W, the size of sweeping droplets appears to be similar. On grate-C I, most of the condensed droplets in the path are swept along with the sliding droplet, leaving the surface area clear of droplets except for a few tiny residual droplets trapped inside grates. A similar feature is also observed on grate-W I. However, on both post-C I and post-W I, several large droplets (~2–3 mm in diameter) remain stuck on the surface even after droplet sweeping, testifying to a much larger pinning force on posts than on grates.

To understand the different condensation behavior between posts and grates or/and between the Cassie state and Wenzel state, a microscopic force analysis is applied to calculate the pinning force at the contact line using the geometric details of surface patterns.

Figure 5 shows a schematic illustration of the contact line force acting on a droplet when the droplet begins to slide on each surface. To slide on the surface, the droplet should overcome the maximum pinning force imparted by surface structures, which is dependent on the structure shape and wetting state, as detailed in the following text.

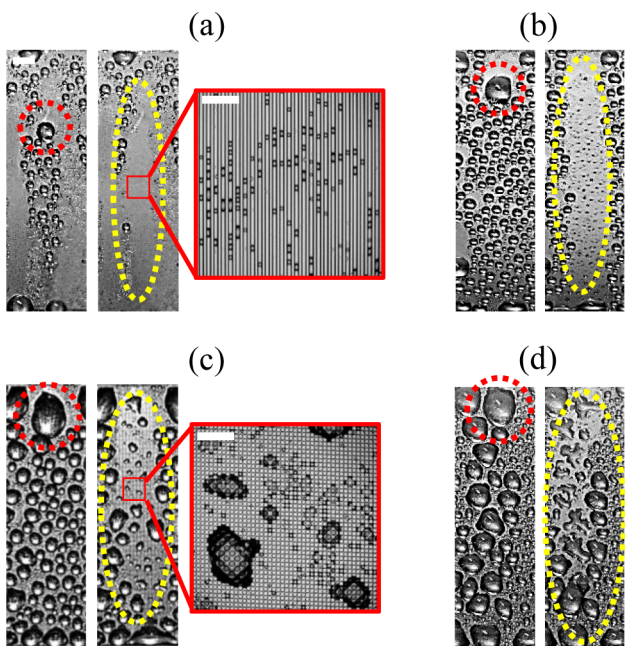


Figure 4. Droplet sliding motion on (a) grate-C I, (b) grate-W I, (c) post-C I, and (d) post-W I. The solid red circles and dotted yellow circles show the sliding droplet and the area swept by the droplet, respectively (scale bar = 2.5 mm). The red rectangle shows the remaining small droplets after the sweeping (scale bar = 0.3 mm).

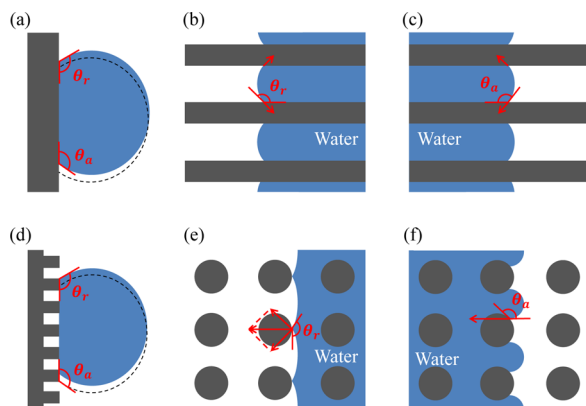


Figure 5. Contact line force acting on a droplet residing on (a–c) grates and (d–f) posts when the droplet begins to slide on the surfaces. (a) Side view of a droplet on the Cassie state grate surface. Top view of the rear (b) and front (c) of a droplet on the Wenzel state grate surface. (d) Side view of a droplet on the Cassie state post surface. Top view of the rear (e) and front (f) of a droplet on the Wenzel state post surface.

Note that some of the condensed droplets might be in a partial Wenzel state (i.e., intermediate state between Cassie and Wenzel states) instead of complete Cassie or Wenzel states. However, for simplicity, we consider only the complete Cassie or Wenzel state in this study.

On grate-C surfaces, it is expected that the droplet interacts only with the top of the structures because of the vapor layer underneath. So a pinning force per unit length perpendicular to the sliding direction is calculated as follows

$$F_{C,\text{grating}} = F_{\text{top}} = \frac{W\gamma(\cos \theta_r - \cos \theta_a)}{L} \quad (1)$$

where W is the width of the grates, γ is the surface tension of the liquid–gas interface, and L is the center-to-center distance of structures (i.e., defined as pitch). On grate-W surface, the droplet makes additional contact with the side wall and bottom surfaces as well as the top surface and, accordingly, the pinning force per unit length increases over grate-C surfaces with additional resistance from the side wall and bottom area as given below.

$$\begin{aligned} F_{W,\text{grating}} &= F_{\text{top}} + F_{\text{side wall}} + F_{\text{bottom}} = \frac{w\gamma(\cos \theta_r - \cos \theta_a)}{L} \\ &+ \frac{(L-w)\gamma(\cos \theta_r - \cos \theta_a)}{L} + \frac{2H\gamma(\cos \theta_r - \cos \theta_a)}{L} \\ &= \frac{\gamma(2H + L)(\cos \theta_r - \cos \theta_a)}{L} \end{aligned} \quad (2)$$

where H is the grate height.

A similar analysis can be applied to posts, although the mechanism of sliding is slightly different on posts because the receding contact line of a water droplets needs to be continuously detached from each post to advance to the next one as shown by prior studies^{37,38} and the contact line at the front advances by touching the next post because of a large contact angle in the front. Therefore, on post-C surfaces, the resistance force per unit length perpendicular to the sliding direction is solely determined by the receding contact line and is given by the following equation³⁷

$$F_{C,\text{post}} = F_{\text{top}} = \frac{\pi D\gamma \cos \theta_r}{L} \quad (3)$$

where D is the diameter of the post. On post-W surfaces, the contact line forces on the side wall and bottom of the structures would make an additional contribution to the overall resistance. However, unlike grate-W surfaces, the droplet needs to experience a series of depinning processes from each post to advance to the next one. Although the depinning process is three-dimensional in nature, we simplify the contact line movement as one-dimensional while calculating the change in the pinning force with the contact line movement. Then, the maximum pinning force during the contact line movement is considered to be the resistance that the droplet should overcome to slide over the surface as shown in Figure 5. On post-W surfaces, the overall resistance per unit length is given as the following equation.

$$\begin{aligned} F_{W,\text{post}} &= F_{\text{top}} + F_{\text{side wall}} + F_{\text{bottom}} \\ &= \frac{\pi D\gamma \cos \theta_r + 2H\gamma(1 + \sin \theta_r) + L\gamma(\cos \theta_r - \cos \theta_a)}{L} \end{aligned} \quad (4)$$

The diameter of a sliding droplet can be calculated by equating the pinning energy to the gravitational energy when a droplet moves by dl on a vertical surface.³² Here the energy associated with a downward direction by a gravitational force is given by $W_g = \rho g V dl$, and the energy associated with the pinning force is given by $W_c = bk dl$, resulting in the sliding condition of $\rho g V \geq bk$, where m is the mass of a droplet, g is the gravitational acceleration, V is the volume of a droplet, and b is the contact diameter of the droplet, as shown in Figure 6. Here, k is a numerical constant known as the retentive force factor and corresponds to the calculated resistance force F in the above analysis.

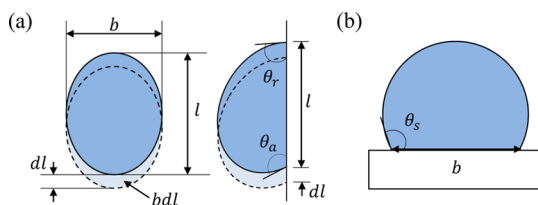


Figure 6. Schematic illustration of (a) a sliding droplet and (b) a spherical droplet on a surface.

Assuming that the droplet maintains a spherical cap shape, the volume of the droplet can be expressed as a function of the contact diameter and contact angle.

$$V = \frac{\pi b^3}{24} (2 \csc^3 \theta_s - 3 \cot \theta_s \csc^2 \theta_s + \cot^3 \theta_s) \quad (5)$$

By applying the above equations to tested surface structures, we could calculate the total pinning forces between a droplet and each surface for two wetting states as shown in Figure 7.

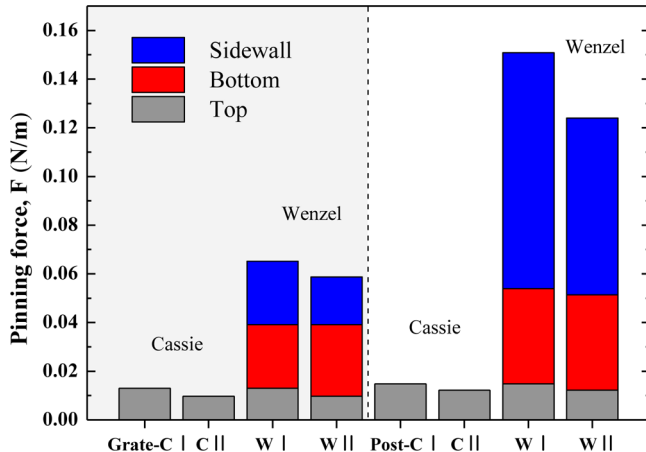


Figure 7. Calculated total pinning forces on each surface. The pinning force of the Wenzel state is larger than that of the Cassie state by additional contributions from the bottom wall (red) and side wall (blue).

From this graph, we can evaluate the degree of pinning force on each contacted area and compare the total pinning force of each sample. First, the total pinning force of the Wenzel state surfaces including top, side wall, and bottom pinning forces are larger than that of the Cassie state surfaces that just have the top pinning force. (The pinning forces of the Wenzel state are larger than those of the Cassie state by about 5–6 times in grate surfaces and about 19 times in post surfaces.) Second, in the Wenzel state, the total pinning force of the post surfaces having a round side wall is larger than the grate surfaces having a parallel side wall by about 2-fold. Considering only the pinning forces of the sidewall, we found that the round-shaped post structures have a larger pinning force than the parallel-shaped grates by about 3–4-fold.

Figure 8 compares the predicted sliding droplet diameters from the above calculation with those actually observed in the experiments, which exhibits good agreement between the prediction and the experiment for grates. However, for posts, the actual sliding droplet size on post-C surfaces is much larger than the prediction and is comparable to that on post-W surfaces, which implies that the droplets are not in the Cassie state.

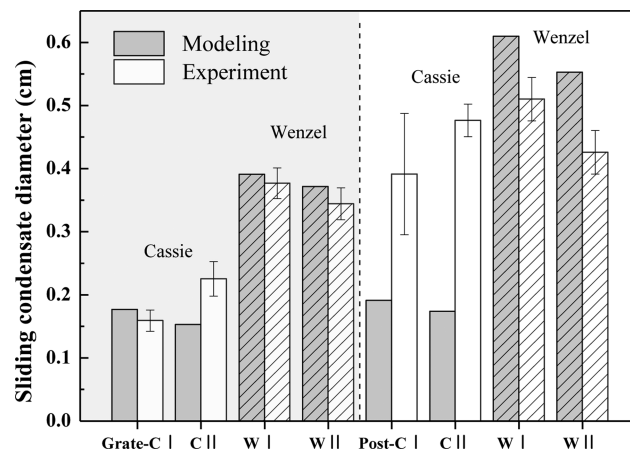


Figure 8. Sliding droplet diameters calculated by modeling and observed by experiments. Good agreement between modeling values and experimental results is observed, except for the Cassie state post surfaces.

state on post-C surfaces and the wetting criteria based on E^* might be inapplicable to posts.

3.2. Wetting States during Condensation. To understand further the condensation behavior and the resultant wetting state on each surface, we employed optical microscopy to determine the actual wetting state on the microscale by focusing through the droplets. For the Wenzel droplets, there is no light-refracting interface between the droplets and surface, which allows us to see the surface patterns clearly. For the Cassie droplets, however, the liquid–air interface refracts light and surface patterns look blurred. As shown in Figure 9a, the droplets on most surfaces initially show satisfactory agreement with the expectation of the wetting state by the E^* criteria. However, the droplets on the post-C I surface begin to spread out irregularly at 50 min and begin to adopt a similar morphology to that on the post-W I surface after 70 min, indicating that the droplet is no longer in the Cassie state.

Figure 9b shows time-lapse images of droplets coalescing on the grate-C I and post-C I surfaces. When two condensates merge on the surfaces, some parts of the droplet can penetrate the structures because surface energy released during merging is converted to fluctuations³⁹ or kinetic energy,⁴⁰ which provide sufficient energy for the transition from the Cassie state to the Wenzel state if the structures are not tall enough compared to the merged droplet.¹⁰ On the grate-C I surface, the liquid–solid interface elongates along the direction of the grates during merging, and the droplet vibrates along the same direction because of the difference in the energy barrier along and across grates. Later, the pinned interface returns to the top of grates, and the droplet relaxes to a more spherical shape, implying the occurrence of a dewetting transition from the Wenzel to the Cassie state. Meanwhile, on the post-C I surface, the liquid–solid interface does not return to the top of posts after penetrating structures with no sign of the transition from the Wenzel state to the Cassie state on posts, even when the Cassie state is an energetically more stable state. The spontaneous dewetting transition from the Wenzel state to the Cassie state on grates was experimentally demonstrated in the previous studies, after the transition from the Cassie state to the Wenzel state was intentionally triggered by electrowetting.^{41,42} Meanwhile, there is no known example of the spontaneous transition from the Wenzel state to the Cassie state on posts. Only when

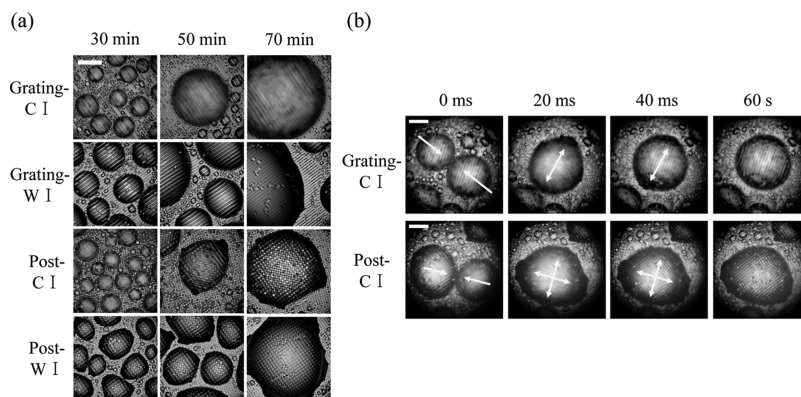


Figure 9. (a) Time-lapse microscopy images of the condensed droplets on grate-C I, grate-W I, post-C I, and post-W I surfaces. On the post-C I surface, the droplets do not remain in the Cassie state after 70 min. (b) Time-lapse images of the droplets coalescing on grate-C I and post-C I surfaces. After the droplets merge, their returns to the round shape on the grate-C I surface with recovery of the Cassie state. However, on the post-C I surface, the droplet is pinned into structures upon transitioning to the Wenzel state (scale bar = 0.6 mm).

the external energy is supplied to the droplet (e.g., thermal vaporization of the trapped water), the droplet could return to the Cassie State.⁴³ This difference was attributed to the different dynamic pathway from the Wenzel state to the Cassie state between posts and grates.⁴² It has been suggested that a large energy barrier prevents the transition from the Wenzel to the Cassie state on posts, whereas it is absent or is negligibly small on grates.

To capture the different dynamic wetting characteristics between posts and grates, we calculated the energy change during the transition from the Wenzel state to the Cassie state. For simplicity, a three-dimensional meniscus curvature and local contact angle were ignored in calculations. Also, we considered only the change in the surface energy without further considering the kinetic energy and viscous dissipation. As shown in the schematic in Figure 10, we calculated the surface energy change when a unit cell of surface pattern was dewetted from water, while the contact line moved laterally.

On posts, when water moves from (i) to (ii) in Figure 10, the total surface energy change with the moving distance x is given by

$$E_{\text{post}(i \rightarrow ii)} = \gamma(1 + \cos \theta_a)Lx \quad (0 \leq x \leq L - D) \quad (6)$$

Also, when the water advances from (ii) to (iii) as shown Figure 10, the total surface energy varies with the distance x as

$$\begin{aligned} E_{\text{post}(ii \rightarrow iii)} &= \gamma(1 + \cos \theta_a)\{Lx - R^2(\theta' - \sin \theta' \cos \theta')\} \\ &\quad + \gamma \cos \theta_a(2R\theta'H) \quad (L - D < x \leq L) \end{aligned} \quad (7)$$

where R is the radius of the post, θ' is the angle that the liquid–vapor makes with the side wall, and H is the height of the structures (Figure 10).

Meanwhile, as the liquid–vapor interfaces move along the grates, the surface energy change is given by the following equation.

$$E_{\text{grating}} = \gamma(1 + \cos \theta_a)(L - W)x + 2\gammaH \cos \theta_a \quad (8)$$

Here, W is the width of the grates.

Figure 11 graphically shows the surface energy change during the transition from the Wenzel to Cassie state on posts and grates. It can be seen that even when the Cassie state is energetically stable compared to the Wenzel state ($E^* < 1$), the energy barrier would prevent the spontaneous transition from the Wenzel state to the Cassie state on posts, whereas on grates

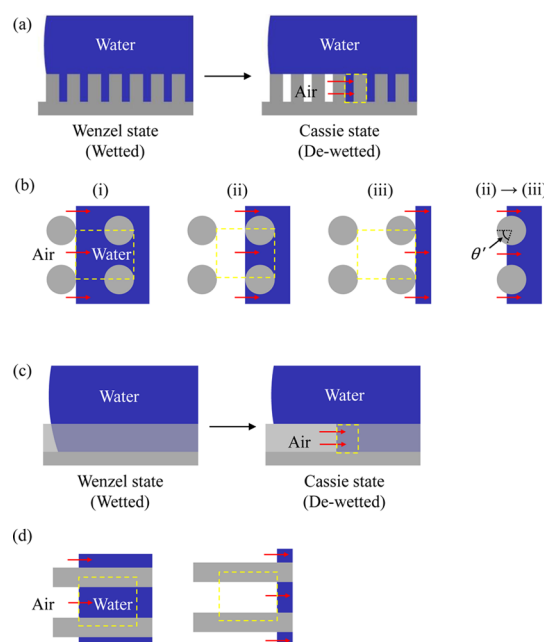


Figure 10. Schematic illustration of the Wenzel to Cassie transition on (a, b) post and (c, d) grate surfaces to calculate the surface energy change with the moving distance x . (a) Side view of the Cassie to Wenzel transition on the Cassie posts. (b) On posts, when the water moves from (i) to (ii), the liquid–vapor interface moves from one post to another. And the interface goes through a space between two posts when the water moves from (ii) to (iii). θ' is the angle that the liquid–vapor makes with the side wall. (c) Side view of the Cassie to Wenzel transition on the Cassie grates. (d) When the Wenzel is transitioned to the Cassie state on grates, the water moves only in the direction along the grates. Yellow squares are the unit volumes, and we determined that they comprise a local energy barrier.

no energy barrier is present when the Wenzel state transitions to the Cassie state. On posts, our calculation predicts that the energy barrier would decrease as the ratio of the post diameter to pitch increases or the surface hydrophobicity increases but would never disappear. In line with this prediction, spontaneous dewetting has never before been observed on posts. Also, it is worth mentioning that the forced transition from the Wenzel state to the Cassie state using vibrational energy was reported only on multiscale posts with the

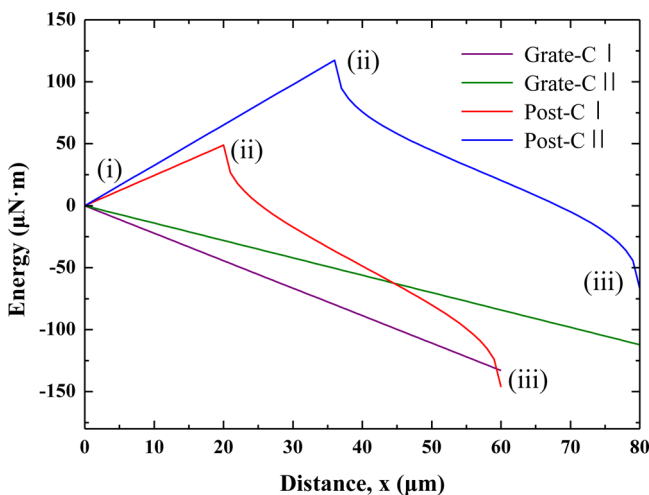


Figure 11. Energy change during the Wenzel to Cassie transition illustrated in Figure 10. The energy barrier in the pathway from the Wenzel to Cassie transition exist on the post surfaces between (i) and (ii).

nanostructured SHPo surface, for which a large contact angle on the surface helped to decrease the energy barrier according to our calculation.⁴⁴ Despite several assumptions made during the calculations, our results qualitatively show that grates are more advantageous in terms of thermodynamic energy barrier in triggering the dewetting transition from the Wenzel state to the Cassie state compared to posts. In actual cases, the energy barrier from the Wenzel state to the Cassie state might be larger than the present calculation results because of additional resistance such as the contact line pinning from surface heterogeneities.

3.3. Water-Harvesting Performance. We investigate how the difference in the droplet mobility and wetting state (i.e., the Cassie and Wenzel states) of SHPo surfaces affects the water-harvesting performance. To compare the harvesting characteristics, the average mass and falling frequency of droplets detached from each surface were measured, as shown in Figure 12. With the smaller pinning force of droplets on grates than on posts, the harvesting falling frequency is noticeably higher on grates. In addition, the Cassie state grates exhibit a greater falling frequency and a smaller droplet mass range compared to the Wenzel state grate surfaces as a result of the smaller pinning forces in the Cassie state compared to those in the Wenzel state. On posts, all of the tested samples similarly exhibit a low falling frequency and large mass ranges because the condensed droplets are in the Wenzel state, which is associated with the strong pinning force.

The harvesting performance is calculated by multiplying the average droplet mass and falling frequency per unit time. Figure 13 shows the water-harvesting performance of each SHPo surface. Despite the similar surface wettability and roughness factor, the performance of the grate surfaces is noticeably better than that of the post surfaces, and the Cassie state grate shows the best water-harvesting performance among the investigated surfaces. Figure 13 shows that the benefit of the enhanced droplet mobility and the resulting efficient surface refreshment of the Cassie state outweigh its potential drawbacks, that is, parasitic thermal resistance of the air layer underneath the droplets.

The present findings show that, even on the SHPo surfaces with similar wettability and surface roughness, geometric details

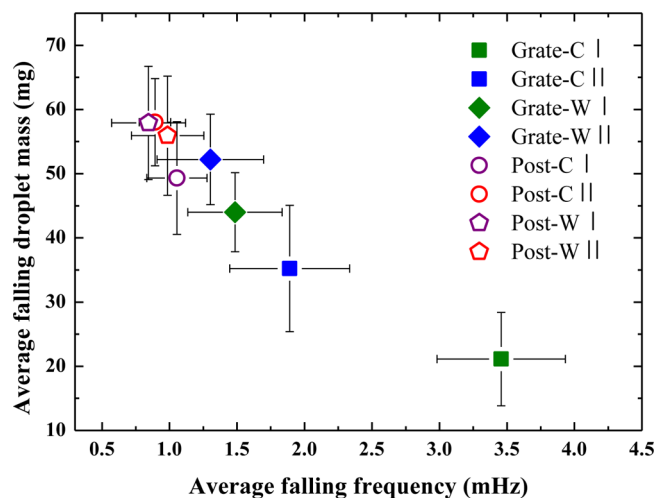


Figure 12. Average mass and falling frequency of droplets detached from each surface. The droplets on the grate surfaces have a wide range of falling frequency and mass. However, the droplets on the post surfaces are collected at the low falling frequency and relatively high mass ranges because of the larger pinning force. In the case of posts, post-C and post-W are indistinguishable because of the occurrence of the Cassie to Wenzel transition on post-C during condensation.

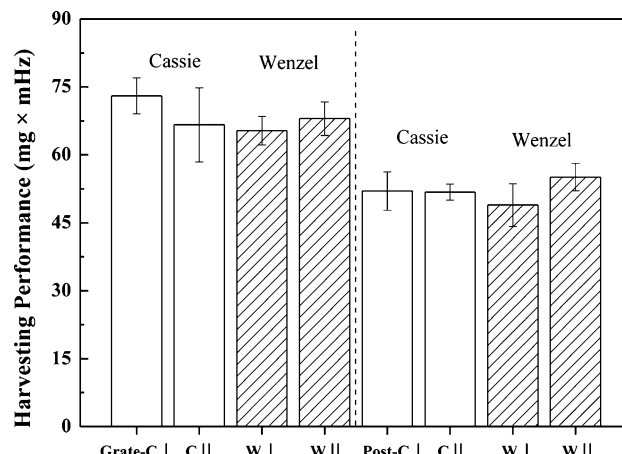


Figure 13. Water-harvesting performance of test surfaces. A higher droplet mobility on grates leads to a better dew-harvesting performance through a faster droplet regeneration and removal process.

have a significant effect on the dew-harvesting performance because of their influence on the dynamic interaction between the droplets and surface structures, as manifested by the distinct droplet wetting state and mobility on tested surfaces in this study. The present results not only ameliorate the understanding of the dynamic interaction between the droplets and the SHPo surfaces during condensation but also help to develop the optimal surfaces for water harvesting via dewing.

4. CONCLUSIONS

We investigated the water-harvesting performance of SHPo with two different patterns (posts and grates) by varying structural parameters to understand the influence of the microscopic surface geometry on the harvesting performance while focusing on the importance of the dynamic interaction between the droplets and surface structures during condensation. It was found that the thermodynamic energy criterion

could be applied to determine the observed wetting state between the Cassie and Wenzel states on grates during condensation but it failed to predict the actual wetting state on posts. This difference between grates and posts was attributed to the different energy barrier in transitioning from the Wenzel state to the Cassie state, i.e., on posts, the energy barrier prevents the transition from the Wenzel state to the Cassie state, but on grates, the droplet is allowed to transition to the Cassie state because of the negligibly small or absent energy barrier. We measured both the mass and frequency of each fallen droplet in a temperature-/humidity-controlled environment to clarify the relationship between the droplet dynamics and water-harvesting performance. This work shows that the different wetting state imparts a different pinning force against droplet movement and thus affects the average mass and falling frequency of collected droplets, which are the crucial factors in harvesting the water from dew. In the present study, the grates in the Cassie state with the highest droplet mobility exhibited the best harvesting performance among the tested surfaces because of the facilitated removal of smaller droplets from the surface.

AUTHOR INFORMATION

Corresponding Authors

*Phone: +82-2-300-0292. E-mail: clee@kau.ac.kr.
*Phone: +82-31-201-3652. E-mail: ysnam1@knu.ac.kr.

Notes

The authors declare no competing financial interest.

ACKNOWLEDGMENTS

This research was supported by the Basic Science Research Program through the National Research Foundation of Korea (NRF) funded by the Ministry of Science, ICT & Future Planning (no. 2012R1A1A1014845).

REFERENCES

- (1) Beér, J. M. High efficiency electric power generation: The environmental role. *Prog. Energy Combust.* **2007**, *33*, 107–134.
- (2) Khawaji, A. D.; Kutubkhana, I. K.; Wie, J.-M. Advances in seawater desalination technologies. *Desalination* **2008**, *221*, 47–69.
- (3) Pérez-Lombard, L.; Ortiz, J.; Pout, C. A review on buildings energy consumption information. *Energy Build.* **2008**, *40*, 394–398.
- (4) Patankar, N. A. Supernucleating surfaces for nucleate boiling and dropwise condensation heat transfer. *Soft Matter* **2010**, *6*, 1613–1620.
- (5) Andrews, H. G.; Eccles, E. A.; Schofield, W. C. E.; Badyal, J. P. S. Three-dimensional hierarchical structures for fog harvesting. *Langmuir* **2011**, *27*, 3798–3802.
- (6) Miljkovic, N.; Enright, R.; Nam, Y.; Lopez, K.; Dou, N.; Sack, J.; Wang, E. Jumping-droplet-enhanced condensation on scalable superhydrophobic nanostructured surfaces. *Nano Lett.* **2013**, *13*, 179–187.
- (7) Boreyko, J. B.; Chen, C. H. Self-propelled dropwise condensate on superhydrophobic surfaces. *Phys. Rev. Lett.* **2009**, *103*, 184501.
- (8) Chen, X.; Wu, J.; Ma, R.; Hua, M.; Koratkar, N.; Yao, S.; Wang, Z. Nanograss micropyramidal architectures for continuous dropwise Condensation. *Adv. Funct. Mater.* **2011**, *21*, 4617–4623.
- (9) Lo, C.-W.; Wang, C.-C.; Lu, M.-C. Spatial control of heterogeneous nucleation on the superhydrophobic nanowire array. *Adv. Funct. Mater.* **2014**, *24*, 1211–1217.
- (10) Enright, R.; Miljkovic, N.; Al-Obidi, A.; Thompson, C. V.; Wang, E. N. Condensation on superhydrophobic surfaces: the role of local energy barriers and structure length scale. *Langmuir* **2012**, *28*, 14424–14432.
- (11) Quéré, D. Non-sticking drops. *Rep. Prog. Phys.* **2005**, *68*, 2495.
- (12) Lafuma, A.; Quéré, D. Superhydrophobic states. *Nat. Mater.* **2003**, *2*, 457–460.
- (13) Bormashenko, E. Wetting transitions on biomimetic surfaces. *Philos. Trans. R. Soc. A* **2010**, *368*, 4695–4711.
- (14) Lee, C.; Choi, C.-H.; Kim, C.-J. Structured surfaces for a giant liquid slip. *Phys. Rev. Lett.* **2008**, *101*, 064501.
- (15) Lee, C.; Kim, C.-J. Maximizing the giant liquid slip on superhydrophobic microstructures by nanostructuring their sidewalls. *Langmuir* **2009**, *25*, 12812–12818.
- (16) Lee, C.; Kim, C.-J. Underwater restoration and retention of gases on superhydrophobic surfaces for drag reduction. *Phys. Rev. Lett.* **2011**, *106*, 014502.
- (17) Lee, C.; Kim, C.-J. Wetting and active dewetting processes of hierarchically constructed superhydrophobic surfaces fully immersed in water. *J. Microelectromech. Syst.* **2012**, *21*, 712–720.
- (18) Zhang, J.; Han, Y. Dual-parallel-channel shape-gradient surfaces: toward oriented and reversible movement of water droplets. *Langmuir* **2009**, *25*, 14195–14199.
- (19) Yang, J.-T.; Yang, Z.-H.; Chen, C.-Y.; Yao, D.-J. Conversion of surface energy and manipulation of a single droplet across micro-patterned surfaces. *Langmuir* **2008**, *24*, 9889–9897.
- (20) Carlborg, C. F.; van der Wijngaart, W. Sustained superhydrophobic friction reduction at high liquid pressures and large flows. *Langmuir* **2010**, *27*, 487–493.
- (21) Li, X.; Mao, L.; Ma, X. Dynamic behavior of water droplet impact on microtextured surfaces: the effect of geometrical parameters on anisotropic wetting and the maximum spreading diameter. *Langmuir* **2012**, *29*, 1129–1138.
- (22) Lee, J. B.; Lee, S. H. Dynamic wetting and spreading characteristics of a liquid droplet impinging on hydrophobic textured surfaces. *Langmuir* **2011**, *27*, 6565–6573.
- (23) Malik, F. T.; Clement, R. M.; Gethin, D. T.; Krawszik, W.; Parker, A. R. Nature's moisture harvesters: a comparative review. *Bioinspir. Biomim.* **2014**, *9*, 031002.
- (24) Ju, J.; Bai, H.; Zheng, Y.; Zhao, T.; Fang, R.; Jiang, L. A multi-structural and multi-functional integrated fog collection system in cactus. *Nat. Commun.* **2012**, *3*, 1247.
- (25) Nikolayev, V. S.; Beysens, D.; Gioda, A.; Milimouka, I.; Katiushin, E.; Morel, J.-P. Water recovery from dew. *J. Hydrology* **1996**, *182*, 19–35.
- (26) Beysens, D. The formation of dew. *Atmos. Res.* **1995**, *39*, 215–237.
- (27) Comanns, P.; Effertz, C.; Hischen, F.; Staudt, K.; Bohme, W.; Baumgartner, W. Moisture harvesting and water transport through specialized micro-structures on the integument of lizards. *Beilstein J. Nanotechnol.* **2011**, *2*, 204–214.
- (28) Lee, A.; Moon, M.-W.; Lim, H.; Kim, W.-D.; Kim, H.-Y. Water harvest via dewing. *Langmuir* **2012**, *28*, 10183–10191.
- (29) Hugenholtz, P.; Fuerst, J. A. Heterotrophic bacteria in an air-handling system. *Appl. Environ. Microbiol.* **1992**, *58*, 3914–3920.
- (30) Garrod, R. P.; Harris, L. G.; Schofield, W. C.; McGetrick, J.; Ward, L. J.; Teare, D. O. H.; Badyal, J. P. S. Mimicking a Stenocara beetle's back for microcondensation using plasmachemical patterned superhydrophobic–superhydrophilic surfaces. *Langmuir* **2006**, *23*, 689–693.
- (31) White, B.; Sarkar, A.; Kietzig, A.-M. Fog-harvesting inspired by the Stenocara beetle—An analysis of drop collection and removal from biomimetic samples with wetting contrast. *Appl. Surf. Sci.* **2013**, *284*, 826–836.
- (32) Lalia, B. S.; Anand, S.; Varanasi, K. K.; Hashaikeh, R. Fog-harvesting potential of lubricant-impregnated electrospun nanomats. *Langmuir* **2013**, *29*, 13081–13088.
- (33) Furmidge, C. G. L. Studies at phase interfaces. I. The sliding of liquid drops on solid surfaces and a theory for spray retention. *J. Colloid Sci.* **1962**, *17*, 309–324.
- (34) Choi, W.; Tuteja, A.; Mabry, J. M.; Cohen, R. E.; McKinley, G. H. A modified Cassie–Baxter relationship to explain contact angle hysteresis and anisotropy on non-wetting textured surfaces. *J. Colloid Interface Sci.* **2009**, *339*, 208–216.
- (35) Carey, V.P. *Liquid Vapor Phase Change Phenomena*; Taylor & Francis Group: New York, 2007.

- (36) Kim, S.; Kim, K. J. Dropwise condensation modeling suitable for superhydrophobic surfaces. *J. Heat Transfer* **2011**, *133*, 081502–081502.
- (37) Xu, W.; Choi, C.-H. From sticky to slippery droplets: dynamics of contact line depinning on superhydrophobic surfaces. *Phys. Rev. Lett.* **2012**, *109*, 024504.
- (38) Lv, C.; Yang, C.; Hao, P.; He, F.; Zheng, Q. Sliding of water droplets on microstructured hydrophobic surfaces. *Langmuir* **2010**, *26*, 8704–8708.
- (39) Narhe, R.; Beysens, D.; Nikolayev, V. S. Contact line dynamics in drop coalescence and spreading. *Langmuir* **2004**, *20*, 1213–1221.
- (40) Nam, Y.; Kim, H.; Shin, S. Energy and hydrodynamic analyses of coalescence-induced jumping droplets. *Appl. Phys. Lett.* **2013**, *103*, 161601.
- (41) Berry, S.; Fedynyshyn, T.; Parameswaran, L.; Cabral, A. Reversible electrowetting on dual-scale-patterned corrugated microstructured surfaces. *J. Microelectromech. Syst.* **2012**, *21*, 1261–1271.
- (42) Vrancken, R. J.; et al. Fully reversible transition from Wenzel to Cassie–Baxter states on corrugated superhydrophobic surfaces. *Langmuir* **2009**, *26*, 3335–3341.
- (43) Krupenkin, T. N.; Taylor, J. A.; Wang, E. N.; Kolodner, P.; Hodes, M.; Salamon, T. R. Reversible wetting–dewetting transitions on electrically tunable superhydrophobic nanostructured surfaces. *Langmuir* **2007**, *23*, 9128–9133.
- (44) Boreyko, J. B.; Chen, C.-H. Restoring superhydrophobicity of lotus leaves with vibration-induced dewetting. *Phys. Rev. Lett.* **2009**, *103*, 174502.